Magnetic resonance force microscopy for condensed matter

Wagenaar, J.J.T.

2

Experimental setup

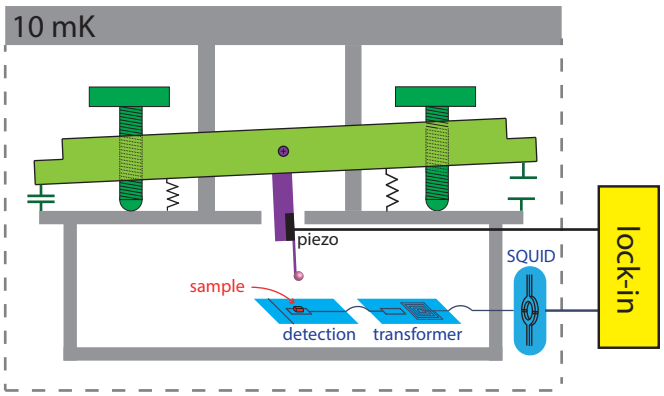

Figure 2.1: This chapter consists of five sections, one for each of the key ingredients of our MRFM setup. Each one is indicated here with a different color.

Our MRFM setup will be discussed in five parts. The first part is about the low vibration cryogen free dilution refrigerator to obtain millikelvin temperatures, which is discussed in Sec. 2.1. Secondly in Sec. 2.2, we discuss the detection chip, which consists of a radio frequency wire and a pickup coil. The pickup coil is connected to a SQUID via a transformer. A magnetic particle is glued to the free end of the cantilever, together forming the most crucial part in the setup, the sensor itself (Sec. 2.3). The cantilever can be positioned above the detection chip using an in-house developed cryopositioning system, see Sec. 2.4. Lastly, we discuss the feedback mechanism, which enables one to readout the cantilever's resonance frequency using the phase locked loop of a lock-in ampli-

fier in Sec. 2.5.

2.1 *Low vibration cryogen free dilution refrigerator*

Most scanning probe techniques gain in sensitivity when performing experiments at cryogenic temperatures. Noise sources, like the Johnson noise in resistors, and the thermal displacement noise of the probe, increase linearly with temperature. For high frequencies, $hf \gg k_B T$, the occupation number of phonons and atomic excitations, which is then smaller than 1, even goes down exponentially with temperature. Therefore, it is useful to perform experiments at temperatures as low as possible.

Conventional cryostats[1] use boiling liquid helium to cool down to a temperature of $1-4$ K. Using ^{3}He, further cooling can be achieved using a number of techniques, where special attention is needed to avoid possible vibrations, caused by pumps and boiling liquids.

[1] Song et al. 2010

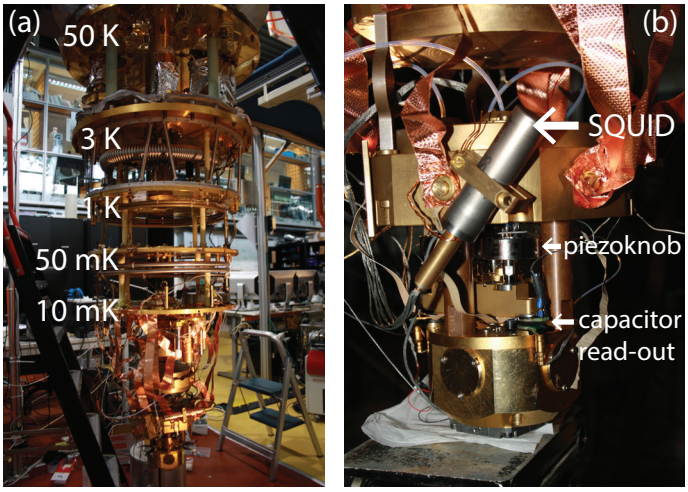

Figure 2.2: **a)** The cryostat when all heat shields are removed. Indicated are the temperatures of the different plates. **b)** A photo of the bottom part of the cryostat, where the experiment is placed. Visible is the magnetic field shielding tube of the SQUID. Furthermore, one of the three piezoknobs is shown, together with one of the capacitor readouts. The detection chip and sample are placed within a niobium foil shielded chamber.

Our cryostat[2] is cooled by a 2-stage pulse tube refrigerator[3]. The use of a pulse tube has the advantage that the helium dewar does not need to be regurarly refilled, and that there is no longer a liquid helium supplier needed[4]. The cooling power of the pulse tube is 36 W at a temperature of 45 K at the first stage, which is connected to the 50K-plate, and 1.35 W at a temperature of 4.2 K, at the

[2] CF-650 by Leiden Cryogenics, The Netherlands.

[3] PT415-RM by Cryomech, United States of America.

[4] Typically 100 liter a week at €10 per liter.

second stage, the 3K-plate. The cryostat also contains a dilution refrigerator to cool down to a base temperature of 10 mK. The cooling power is 650 μW at a temperature of 120 mK. Using the quadratic temperature dependence of the cooling power, this translates to a cooling power[5] of only 5 μW at 10 mK.

[5] Pobell 2007

The use of a pulse tube cooler has some disadvantages, mainly the large forces acting on the cooling stages and the acoustical vibrations due to gas flow. Previous work in our group[6], has shown that these difficulties can be overcome using a number of measures. Here we summarize the measures taken. First the stages of the pulsetube are disconnected from the plates and reconnected with soft copper braiding. Secondly, all plates below the 3K-plate (see Fig. 2.2) are hanging on springs, with an eddy current damper between the 1K- and the 3K-plate. Thirdly, the whole experiment is positioned below a mass spring system, which consists of three large copper masses, connected with stiff springs, together forming a low-pass-filter with a cut-off frequency well below the resonance frequency of the cantilever. All together, these measures were enough to obtain atomic resolution with a scanning tunneling microscope inside a cryogen free dilution refrigerator[7].

[6] Wijts 2013; Den Haan et al. 2014; Den Haan 2016

[7] Den Haan et al. 2014

After preparing the experiment, the heat shields are connected to the 50mK- and 1K-plates, to reduce heat radiation from high temperature plates to the experiment. These shields are covered with superconducting niobium foil to reduce electromagnetic interference. At the 3K-plate, a vacuum compatible shield is placed, which defines the inner vacuum chamber as everything below this plate. An extra heat shield is placed at the 50K-plate, to end with a second vacuum compatible shield at the room temperature plate, defining the outer vacuum chamber as the space between the room temperature plate and the 3K-shield.

After all shields are placed and the inner and outer vacuum chambers are pumped down to a pressure of $< 10^{-2}$ mBar, a few mBar of Helium gas is used as heat exchange gas in the inner vacuum chamber. Hereafter, the

pulse tube can start to cool down the cryostat to < 4 K, which takes approximately 2.5 days.

After the cryostat is cooled down, the exchange gas is removed using carbon sorption pumps. The experiment is now at a temperature of well below 4 K, but the temperature can be further lowered down to 10 mK using the built-in dilution refrigerator. Normally, cooling down from 4 K to approximately 10 mK takes less than half a day.

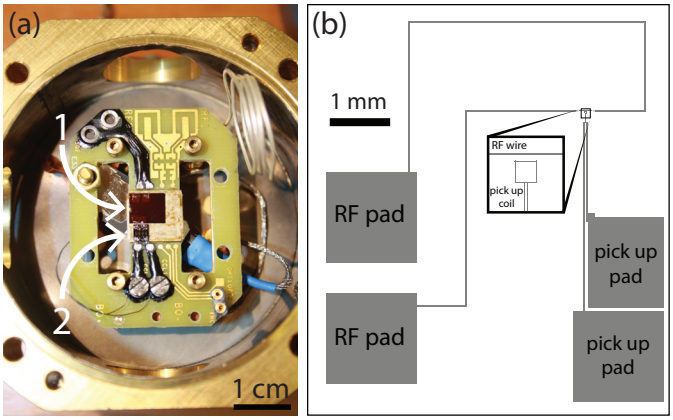

Figure 2.3: **a)** A photo of the sample holder, together with the detection chip and transformer. The experimental chamber is gold plated aluminum, with niobium foil at the inside. The copper sample holder is surrounded by a standard printed circuit board, but glued on top is some niobium foil embedded in stycast for the connection to the radio-frequency wire and transformer/pickup coil. The design of this sample holder is also used for electron spin resonance experiments (Wijts, 2013). 1 indicates the detector chip and 2 indicates the transformer chip. **b)** Sketch of the detection chip with a close up on the pickup coil.

2.2 *Detection of the cantilever's oscillation*

In conventional MRFM setups, the oscillation of the cantilever is detected using a laser interferometer[8]. There are some limitations for MRFM when using optical sensors. The most important one, is that when pushing MRFM to the limit of small force sensors, the optical power needs to be increased for sufficient reflection. But for most materials, the thermal conductivity is small at low temperatures. It was shown by Poggio and Degen (2010) and Mamin and Rugar (2001) that at a laser power of respectively only 20 nW and 2 nW, the temperature of a single-crystal Si cantilever increased from 100 mK to 200 mK. With the used laser power in most experiments, the cantilever temperature did not get below 1 K. Even when laser interferometer techniques would improve, it is possible that the laser

[8] Züger and Rugar 1993; Hammel et al. 1995; Garner et al. 2004; Degen et al. 2009; Poggio and Degen 2010

gives unwanted optical excitations in the sample under study.

In order to overcome this limitation, a superconducting quantum interference device based read-out scheme is implemented[9]. This detection mechanism is based on three ingredients: one is the pickup coil, a single small superconducting loop which can pickup magnetic flux changes when the magnetic particle on the cantilever oscillates (Fig. 2.3b). Secondly, there is the superconducting quantum interference device (SQUID), which can detect flux changes with a very high accuracy. Between the SQUID and the pickup coil, a transformer[10] is placed, which is used to match the input inductance of the SQUID and the output impedance of the pickup coil (visible below the detection chip in Fig. 2.3a). A detailed analysis of the coupling parameters and SQUID theory is given in the previous work of Wijts (2013).

The transformer is connected to the pickup coil using aluminum wire bonds, which become superconducting below its critical temperature of 1.15 K. Above this temperature, the Johnson current noise increases the noise at the SQUID by three orders of magnitude (30 dB). The transformer is connected to the SQUID as follows: first it is wire bonded to niobium foil, which was previously fixated to the printed circuit board with stycast[11]. The niobium foil is pressed against to two niobium titanium wires using a niobium screw. The wires are inside a teflon tube, contained in a lead tube, to prevent electromagnetic interference, since the SQUID is placed outside the niobium shielded experimental chamber.

The pickup coil is made from NbTiN and is 1.0 µm wide and 265 nm thick, as measured with atomic force microscopy (Fig. 2.4). Fabrication details are discussed by Den Haan (2016) . The radio-frequency wire is fabricated simultaneously with the pickup coil, with a width of 2 µm for a 200 µm long section and 20 µm elsewhere.

The NbTiN film has a critical temperature of around 15 K, and is used in the groups of T.M. Klapwijk[12] and A. Endo[13] at the Technical University of Delft. The material is used for detectors in astronomy, for the special property

Detection chip
We call the chip that consists of the radio-frequency wire and pickup coil the *detection chip*.

[9] Usenko et al. 2011

[10] Pleikies et al. 2007

[11] Stycast 2850FT

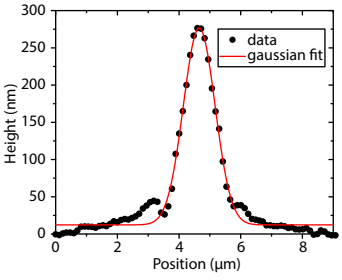

Figure 2.4: A linescan with atomic force microscopy. The linescan is performed at the upper line of the pickup coil along the dashed vertical line in Fig. 2.9b. A Gaussian fit is used to extract a width of 1.0 µm and a height of 265 nm.

[12] Coumou 2015

[13] Thoen et al. 2017

that dissipation in this material is low. For this reason, we started a collaboration with these groups, to achieve low dissipation in our detection chip, especially for the radio-frequency currents we use. For the results presented in this thesis, the currents necessary for saturation experiments were below 1 mA, and gave no observable heating to the sample (Ch. 5).

For the purpose of three dimensional imaging, it is important to be able to apply currents up to several tens of mA, at MHz frequencies. For radio-frequencies of several megahertzs and for currents higher than several milliamps, we observe millikelvin heating of the sample holder temperature at millikelvin temperatures. A calorimeter was designed and used to address this dissipation[14]. However, the origin of the dissipation remains an open question.

[14] Bastiaans 2015

2.3 *Cantilever*

2.3.1 *Geometry bare cantilever*

[15] Poggio et al. 2007; Madsen et al. 2004

[16] Degen et al. 2008

[17] Chui et al. 2003; Mamin et al. 2003

When performing MRFM experiments with the adiabatic rapid passage protocol[15], it was shown by Poggio et al. (2007) that the spin correlation time while rotating the spin, is influenced by the thermal excitation of higher cantilever modes[16]. In order to suppress this effect as much as possible, ultrasoft cantilevers with suppressed thermal motion of higher modes were designed by adding masses at the end of the cantilever[17]. In our setup, the cantilever is used without the mirror, which is used for readout with a laser, and without the masses at the end of the cantilever.

In this work, we use the same cantilever for all experiments. The length, width and thickness are 145 μm, 5 μm and 100 nm respectively. Without the magnetic particle attached, the resonance frequency f_0 is approximately 7 kHz. With the magnetic particle, the resonance frequency is approximatly 3 kHz. The spring constant is $k_0 \approx 7 \times 10^{-5}$ N/m.

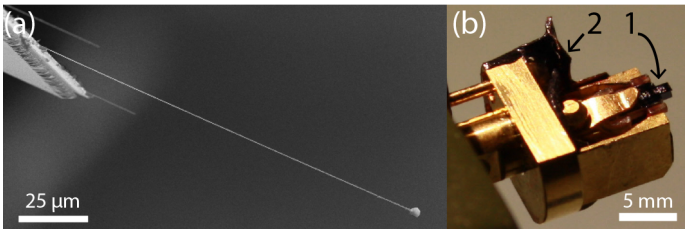

Figure 2.5: **a)** Scanning electron microscopy image of the cantilever with the magnetic particle glued to the free end. **b)** Photo of the cantilever holder. The cantilever chip (1) is held with a clip. On the left you see the stycast (2) which is used to fixate the piezoelectric element to the cantilever holder.

2.3.2 *Magnetic dipole*

In order to "glue" the magnetic particle, we use a nanomanipulator to move the cantilever with nanometer precision in a scanning electron microscope[18]. Using electron beam induced deposition from a platinum containing precursor gas ($Pt(PF_3)_4$), a spherical particle from a commercial NdFeB-powder[19] is attached to the cantilever (Fig. 2.5). The particle has a diameter of 3.43 µm. The saturation magnetization[20] of the material is expected to be $\mu_0 M_r = 1.3 \pm 0.1$ T, which is in agreement with the found saturation magnetization of 1.15 T in Ch. 7.

After the particle is attached, it is magnetized in a field of 5 T. The magnetization is parallel to the direction of the fundamental mode, this gives a maximal possible coupling with a spin in the sample.

[18] Heeres et al. 2010

[19] Magnequench, type MQP-S-11-9

[20] Nazaretski et al. 2009; Vinante et al. 2011a

2.3.3 *Cantilever's transfer function*

The differential equation for a mechanical resonator is given by:

$$m_{eff}\ddot{x} = -k_0 x - \gamma \dot{x} + F_{drive}(t) \tag{2.1}$$

With m_{eff} the (effective) mass of the cantilever, which is for our cantilever 2.0×10^{-13} kg, the stiffness $k_0 = 7.0 \times 10^{-5}$ N/m, x the motion of the cantilever, with the dots representing the time derivatives. γ is the friction of the cantilever, which equals at low temperatures 1.3×10^{-13} kg/s. $F_{drive}(t)$ is the driving force. We can solve this differential equation in the Fourier domain, obtaining the transfer function $H(\omega)$ of the resonator:

Lorentzian fit
For $Q \gg 1$, the transfer function squared can be approximated with a Lorentzian function. For example, if the value $|H(f)|^2$ as function of the frequency $f = \frac{\omega}{2\pi}$ is measured, OriginPro can be used to fit the data with the Lorentzian function $y(f)$:

$$y(f) = \frac{2A}{\pi} \frac{B}{4(f - f_0)^2 + B^2} \tag{2.2}$$

The fitted values correspond to the area $A = \frac{Q_0 f_0 \pi}{2}$, in the case that there are no other prefactors, and $B = \frac{f_0}{Q_0}$.

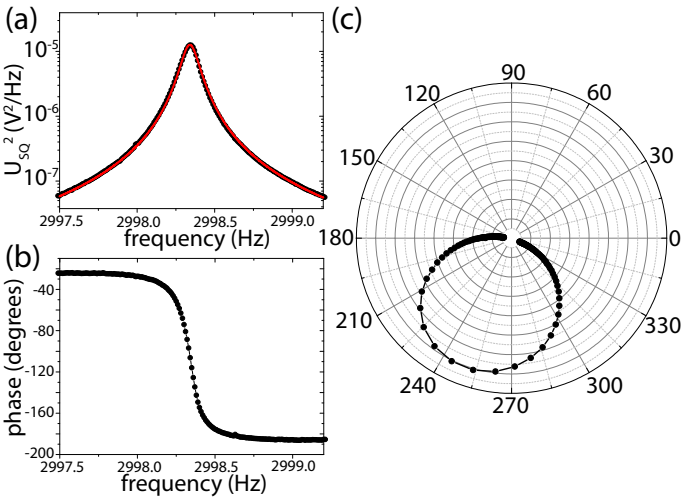

Figure 2.6: **a)** The SQUID's signal squared versus piezo drive frequency, measured using a lock-in. The cantilever is positioned at a height of 25 μm above the center of the pickup coil, see also Fig. 2.9a. The red solid line is a fit according to Eq. 2.2, giving a resonance frequency $f_0 = 2998.340$ Hz, and a quality factor $Q_0 = 2.6 \times 10^4$. **b)** The phase of the SQUID's signal. **c)** A polar plot of the data of a) and b). A resonator gives a characteristic circle. There is an additional phase-shift of 20 degrees due to the various SQUID's signal filters.

$$H(\omega) \equiv \frac{k_0 X(\omega)}{F_{drive}(\omega)} = \frac{1}{1 - \left(\frac{\omega}{\omega_0}\right)^2 + i\frac{\omega}{\omega_0 Q}} \tag{2.3}$$

With $\omega_0 \equiv 2\pi f_0 = \sqrt{\frac{k_0}{m_{eff}}}$, and the quality factor $Q_0 = \frac{m_{eff}\omega_0}{\gamma}$.

2.3.4 *Calibration of the piezoelectric element and cantilever displacement*

The cantilever is driven by the use of a piezoelectric element[21], glued to the cantilever holder. According to the manufacturer's datasheet[22], the displacement of this piezoelectric element as function of voltage has an uncertainty of 20% at room temperature. At cryogenic temperatures, the displacement change approximately proportional to the changes in capacitance, which is in the order of a factor 5. Together with load dependent filters before the piezoelectric element, this makes the displacement versus voltage very uncertain. Therefore, we need a calibration of the proportionality ξ between the displacement x of the cantilever versus applied voltage V_{piezo} on the piezoelectric element.

In our setup, we can use two different calibrations. The first is to use a calibration coil, which is a chip that can

[21] Piezo Linear Actuator with PICMA Multilayer Technology PL033.30 by Physik Instrumente (PI) GmbH & Co., Germany.

[22] Physik Instrumente 2016

be connected between the transformer and the SQUID. This chip can bring a flux into the pickup coil, driving the cantilever, which itself generates a flux again. By measuring the total signal in the SQUID, one can determine the coupling strength between pickup coil and cantilever[23]. Together with the SQUID sensitivity, information about the (mutual) inductance of the different circuits in the detection, and the cantilever's stiffness, one can relate the SQUID's signal to the displacement of the cantilever. This method is quite cumbersome and may be inaccurate in the presence of crosstalk. A second disadvantage is that the calibration coil directly couples with the SQUID, and may therefore add noise to our signal.

[23] Wijts 2013

Therefore, we use the second method, which takes a longer measurement time, but is more straightforward. Since the cantilever is only very soft in one direction, one can use the equipartition theorem[24] to calculate the average mean squared displacement due to thermal fluctuations:

$$\frac{k_0 \langle x^2(t) \rangle}{2} = \frac{k_B T}{2} \tag{2.4}$$

[24] **Equipartition theorem**
The equipartition theorem relates the average energies of the various degrees of freedom of a system with its temperature. The theorem can be derived using statistical physics (Garrod, 1995, p. 82).

With k_0 the cantilever's stiffness, $x(t)$ the displacement of the cantilever, k_B the Boltzmann constant and T the (effective) temperature. We can assume that for small displacements $x(t)$, the SQUID's signal $U_{SQ}(t)$ is linear with the displacement, so therefore we are interested in the coupling strength $\beta \equiv \frac{dU_{SQ}}{dx}$:

$$\beta^2 = \frac{k_0 \langle U_{SQ}^2(t) \rangle}{k_B T} \tag{2.5}$$

We measured $\langle U_{SQ}^2(t) \rangle$ as function of several temperatures of the mixing chamber, see Fig. 2.7.

At low temperatures, the cantilever's temperature T_c saturates due to all possible heating sources and poor heat conductivity between the cantilever and the mixing chamber[25], resulting in:

$$\langle U_{SQ}^2(t) \rangle = \frac{\beta^2 k_B}{k_0} T_c = \frac{\beta^2 k_B}{k_0} \left(T^n - T_0^n \right)^{1/n} \tag{2.6}$$

[25] Usenko et al. 2011

Here T_0 is called the saturation temperature, and T is the temperature of the mixing chamber, which act as the heat

bath for the cantilever. n is an exponent, which is expected to be $n \approx 4$ for thermal boundary resistance and $n \approx 3.5 - 4$ in the case of phonon-mediated bulk transport[26]. From the fit in Fig. 2.7, we find a saturation temperature of $T_0 = 134 \pm 12$ mK, which is much larger than the value $T_0 = 25 \pm 1$ mK found in previous experiments, where a similar cantilever is used. The exponent is fitted $n = 4 \pm 3$.

[26] Rosenberg 1954; Pobell 2007

In our setup, we paid no special attention in good thermalization of the cantilever holder to the mixing chamber. Assuming that we do not have additional heat sources compared with previous experiments, our result implies that not the phonon-mediated bulk transport in the silicon cantilever is the limiting factor, but the thermalization of the cantilever holder.

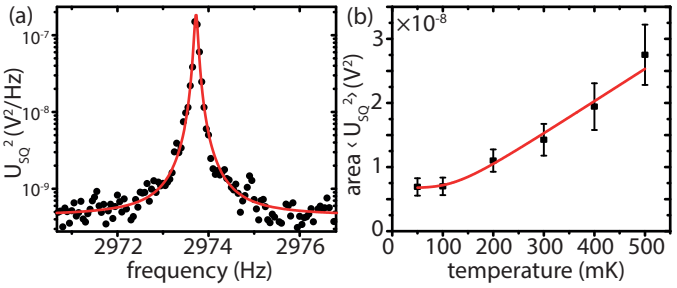

Figure 2.7: **a)** Single thermal spectrum of the cantilever at a temperature of 500 mK. The red solid line is fit with Eq. 2.2 with an additional background signal. **b)** The area of the thermal spectrum $\langle U_{SQ}^2(t) \rangle$ versus temperature, calculated by summation of the Fourier Transform of the SQUID signal and subtraction of the background noise. Each data point represents the mean of at least 36 thermal spectra with the standard deviation as error bar. The red line is a fit according to Eq. 2.6.

Besides the measurement of the thermal spectra, we need to measure $\langle U_{SQ} \rangle$ as function of drive amplitude of the cantilever U_{piezo}, in the region that the displacement is much more than the thermal displacement, to extract the ratio $\frac{dU_{SQ}}{dU_{piezo}}$. Combining this with β, we extract the proportionality of interest ξ:

$$\begin{aligned} \xi &\equiv \frac{dx}{dU_{piezo}} = \frac{dx}{dU_{SQ}} \frac{dU_{SQ}}{dU_{piezo}} \\ &= \frac{1}{\beta} \frac{dU_{SQ}}{dU_{piezo}} \end{aligned} \tag{2.7}$$

Note that this relation includes the transfer function of the cantilever at driving the cantilever at its resonance fre-

quency, since:

$$X(\omega) = H(\omega)X_{piezo}(\omega) \tag{2.8}$$

$$|X(\omega_0)| = Q|X_{piezo}(\omega_0)| \tag{2.9}$$

With Q the quality factor of the cantilever. When the quality factor is altered, ξ will change according to:

$$\xi = \frac{Q}{Q_0}\xi_0 \tag{2.10}$$

With ξ_0 measured far away from the surface and Q the altered quality factor. In our setup, we find typical values of $\xi_0 \approx 10$ nm/mV, depending on the cantilever holder, the used piezoelectric element and wires towards the element.

2.4 *Positioning cantilever*

2.4.1 *Piezoknobs and readout*

The cantilever holder is connected to a brass platform, which itself is held to the experimental chamber with tension springs (Fig. 2.1). The brass platform can be moved in all three dimensions using three piezoknobs[27]. The piezoknobs consist each of a spindle, that can be rotated by piezoelectric elements in the head of the piezoknob. Each torque pulse from the piezoelectric elements rotates the spindle though a stick-slip mechanism. The vertical displacement is in the nm range, while the full range can be several mm.

[27] Janssen Precision Engineering B.V., The Netherlands.

One of the main bottlenecks in our experiments is the reliability of the functioning of the piezoknobs. We experienced that when cooled down, it becomes harder to move the piezoknobs after several weeks of usage. We came up with possible reasons for this malfunctioning. One is that (water) gas in the IVC freezes to solid (ice), freezing solid the piezoknobs. A second possibility was that the platform at which the piezoknobs push was giving too much friction. A third possible reason was that the platform itself together with the springs becomes too stiff. And the last reason is that the friction between the spindle and the nut increases due to wear. After various tests, we

concluded that it is the last that is causing the problems. After time, and possible only below 1 K, the material of the spindles and nut starts to erode, causing small particles which block the smooth motion of the piezoknob. The company[28] is currently improving the spindle and nut.

[28] Personal communication with Huub Janssen, 2016.

The displacement for each torque pulse is not constant, therefore we need a readout mechanism for the position of the cantilever. For this, we use three capacitor sensors. The mechanism is based on the capacitance between two parallel plates; for each sensor, one is connected on the brass platform, and one to the experimental chamber (see Fig. 2.1).

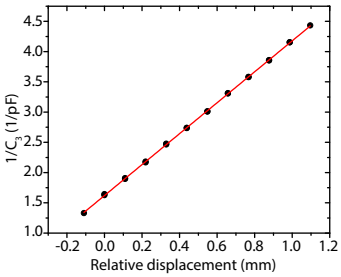

Figure 2.8: We calibrate the position sensors by measuring the capacitance of the position sensors versus distance between the plates. By rotating the piezoknobs manually, the displacement can be determined accurately. The red line is a linear fit according to Eq. 2.11, with an offset capacitance taken into account. We find for sensor 3 an effective area of 44.0 ± 0.1 mm^2.

[29] Griffiths 1999

For two parallel plates in vacuum, where the distance between the plates is smaller than the area of the plates, one can use the Gaussian pill box[29] to determine the capacitance C :

$$C = \frac{\epsilon_0 A}{d} \tag{2.11}$$

With A the area of the smallest plate, d the distance between the plates, and $\epsilon_0 \approx 8.85 \times 10^{-12}$ F/m the vacuum permittivity.

Figure 2.8 shows the calibration of a capacitance sensor. One full turn of all piezoknobs, moves the platform 250 µm. By measuring the capacitance, one can fit Eq. 2.11, taking into account a constant stray capacitance in parallel to the varying capacitance. With the fit, we extract the effective area A for each sensor.

When the distance between the three parallel plates is known, one can use the exact geometry of the setup to calculate the relative position of the cantilever. This calculation is well described by Den Haan (2016). The position we calculate with this method is not accurate enough to determine the position with respect to the center of the pickup coil, which we describe in the next section. Relative displacements can be calculated with sub-µm precision.

2.4.2 *Determining cantilever position relative to pickup coil*

The cantilever needs to be close, within approximately 100 μm with respect to the center of the pickup coil, in order to detect the cantilever's motion above the noise of the SQUID or, when driving the cantilever with a piezoelectric element, above the crosstalk from the piezoelectric element to the SQUID.

At room temperature, we use an optical microscope to position the cantilever within approximately $20 - 30$ μm to the pickup coil, using the three piezoknobs. If the thermal drift during cool down is larger than 100 μm, then this must be compensated for[30].

[30] Wijts 2013

One can use the coupling strength $\beta \equiv \frac{dU_{SQ}}{dx}$ to estimate the absolute position of the cantilever with respect to the center of the pickup coil. Since there are some coupling factors in between the flux change in the pickup coil and the measured flux change in the SQUID, as discussed before, we use a proportionality between the coupling strength and the flux change in the pickup coil:

$$\beta \propto \frac{d}{dx} \iint_S \boldsymbol{B}(\boldsymbol{r}) \cdot d\boldsymbol{S} = \frac{d}{dx} \iint_S B_z(\boldsymbol{r}) dS \tag{2.12}$$

With $\boldsymbol{B}(\boldsymbol{r})$ the magnetic field of the cantilever at position $\boldsymbol{r}$ and S the surface enclosed by the pickup coil. In the last line we used $d\boldsymbol{S} = dS\hat{z}$.

Equation 2.12 can easily be calculated using Matlab or Mathematica. By sweeping the cantilever through its resonance frequency, visible in Fig. 2.6, the signal strength (an additional prefactor in Eq. 2.2) can be extracted. This signal strength is proportional to the absolute value of the coupling strength β. The sign of the coupling strength can be extracted by observing the polar plot (Fig. 2.6c). When the cantilever is positioned near an edge of the pickup coil perpendicular to the direction of the fundamental mode of the cantilever, we see that the coupling factor has a 180 degree phase shift. This phase shift can be used to determine the position of the pickup coil in one dimension with a good accuracy, as is visible in Fig. 2.9.

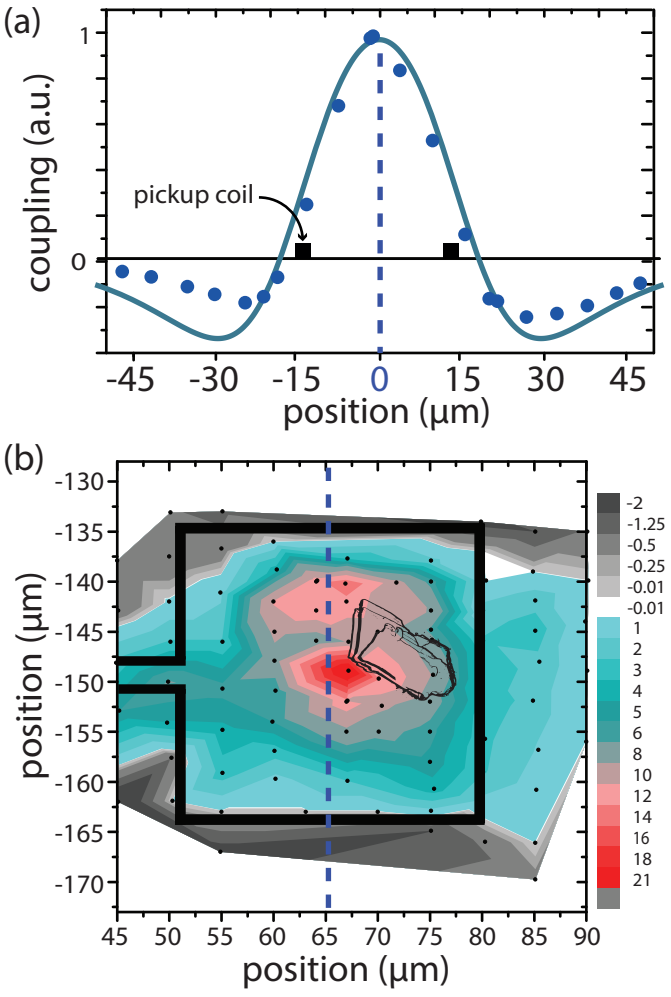

Figure 2.9: **a)** The coupling strength obtained after fitting the response in the SQUID while driving the cantilever versus the position of the cantilever with respect to the pickup coil at a height of 25 μm. The blue solid line is the calculated signal with an added prefactor. From the maximum, one can obtain the absolute position of the center of the pickup coil, for this measurement in one dimension. **b)** The coupling strength (a.u.) while scanning in two dimensions at a height of approximately 15 μm. For this measurement, the coupling strength was influenced by interaction with the BiTe sample (indicated with the thin black lines), that was placed within the pickup coil (indicated with the thick black line), preventing a reliable fit with the calculated signal as obtained in a). The blue dashed line indicates the position at which a) is measured with respect to the pickup coil, but then with a different sample.

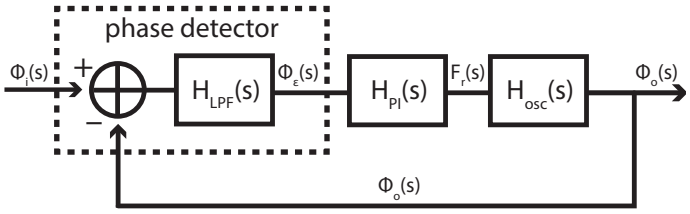

Figure 2.10: Feedback scheme for the phase locked loop circuit of the Zurich Instruments. $\Phi_i(s)$ is the incoming phase which needs to be kept constant. This phase is detected using a phase detector and filtered using a low pass filter with transfer function $H_{LPF}(s)$. The new drive frequency f_r is calculated using PI-feedback, characterized with the transfer function $H_{PI}(s)$. Finally, the internal oscillator sends a new drive frequency to the resonator, which we would like to keep at a constant phase. This frequency can be translated to the phase $\Phi_o(s)$. The phase detector calculates the phase error $\Phi_\epsilon(s)$.

2.5 *The phase locked loop*

The measurements performed in this thesis rely mostly on the detection of shifts in the resonance frequency of the cantilever. Figure 2.6b shows that the slope of the phase is highest when driving the cantilever at its resonance frequency. A phase locked loop (PLL) of a lock-in can use this characteristic to keep the cantilever oscillating at its resonance frequency, meanwhile recording the resonance frequency accurately to determine any frequency shifts during the experiments.

In this section we will give an analysis of the PLL circuit we use[31] to drive the cantilever and detect its resonance frequency. We try to understand the choices the software makes in choosing its settings for the PLL.

Figure 2.10 shows the feedback scheme to keep the phase of the resonator at a fixed value, by changing the drive frequency $f_r(t)$. We assume that the phase at the resonance frequency is a characteristic that remains constant during the measurement[32]. This results in that $f_r(t)$ equals to the resonance frequency $f_0(t)$ of the cantilever.

[31] **Zurich Instruments:**
We use the lock-in version HF2LI of Zurich Instruments, whose specifications can be found in Zurich Instruments AG (2016).

[32] For example, it is imaginable that as a function of time the phase of the voltage that drives the piezoelectric element gradually changes because of a temperature dependent resistance in an RC filter before the piezoelectric element.

2.5.1 *Theory of the phase locked loop feedback scheme*

The feedback scheme works as follows: A phase detector is used to determine the incoming phase of the signal with respect to a reference signal. For simplicity we denoted the incoming signal and reference signal already as a phase signal, $\phi_i(t)$ and $\phi_o(t)$ respectively. In order to remove high frequency noise, the difference signal is filtered using a low pass filter with transfer function $H_{LPF}(s)$. We call the resulting signal the error phase signal $\phi_\epsilon(t)$.

From the error signal $\phi_\epsilon(t)$, the set-point phase is subtracted, but we are only interested in the frequency response of the system, so we can assume this set-point equals zero. The error signal is used to determine the new drive frequency according to the following proportional-integral feedback[31]:

$$f_r(t) = f_c + K_p \left(\phi_\epsilon(t) + \frac{1}{T_i} \int_t \phi_\epsilon(\tau) d\tau \right) \tag{2.13}$$

$$F_r(s) = K_p \left(\Phi_\epsilon(s) + \frac{\Phi_\epsilon(s)}{sT_i} \right) \tag{2.14}$$

The second line is the Laplace Transform[33] of the first with s a complex number frequency parameter. K_p is the proportional feedback in [Hz/degree], T_i the integration time in [s], and f_c is the center frequency, for which it is convenient to equal it to $f_r(0)$. From this, we can define the transfer function of the PI-controller $H_{PI}(s)$:

$$H_{PI}(s) \equiv \frac{F_r(s)}{\Phi_\epsilon(s)} = K_p \left(1 + \frac{1}{sT_i} \right) \tag{2.16}$$

In reality, the PI-controller has a voltage as output, which is given to the oscillator in the lock-in which converts it to a frequency (voltage controller oscillator), but this would only add a proportional gain, which is set to 1 in the software of the lock-in of Zurich Instruments[34]. In order to convert the new frequency to a new reference phase, we use the relation between phase and frequency:

$$\phi_o(t) = \phi_o(0) + \int_0^t \omega(\tau) d\tau \tag{2.17}$$

$$\Phi_o(s) = \frac{2\pi}{s} F_r(s) \qquad \text{[rad/Hz]} \tag{2.18}$$

$$\Phi_o(s) = \frac{360}{s} F_r(s) \qquad \text{[degree/Hz]} \tag{2.19}$$

$$H_{osc}(s) \equiv \frac{\Phi_o(s)}{F_r(s)} = \frac{360}{s} \qquad \text{[degree/Hz]} \tag{2.20}$$

We can now evaluate the feedback scheme by writing down the open transfer function $H_{open}(s)$ of the system[35]:

$$H_{open}(s) = H_{LPF}(s) H_{PI}(s) H_{osc}(s) \tag{2.21}$$

And for the closed loop transfer function $H_{closed}(s)$ we

[33] **Laplace Transform:**
The Laplace transform $X(s)$ of a function $x(t)$ is given by:

$$X(s) = \int_0^\infty x(t) e^{-st} dt \tag{2.15}$$

[34] **Zurich Instruments**
The software of the Zurich Instruments HF2LI (release 12.08.1.17792) offers an Advisor for the PLL settings. Unfortunately, the software specifications does not explain the procedure in detail (Zurich Instruments AG, 2016). But by comparing our result with the numerical results of the Advisor, we can verify their procedure. We find for a first order low pass filter perfect agreement when we divide $H_{PI}(s)$ by a factor of 2.

[35] Wagenaar 2015

find:

$$H_{closed}(s) = \frac{H_{open}(s)}{1 + H_{open}(s)} \tag{2.22}$$

To evaluate this result, we need to specify the low-pass filter. Normally a high order low pass filter is used, but to compare our analysis with the analysis performed in the software of Zurich Instruments[34], we take a simple first order low pass filter:

$$H_{LPF}(s) = \frac{1}{1 + \frac{s}{2\pi f_{LPF}}} \tag{2.23}$$

When we combine Eqs. 2.21 and 2.23 we obtain:

$$H_{open}(s) = \frac{360}{s} K_p \left(1 + \frac{1}{sT_i}\right) \left(\frac{1}{1 + \frac{s}{2\pi f_{LPF}}}\right) \tag{2.24}$$

From which also $H_{closed}(s)$ follows.

2.5.2 *Example of the phase locked loop transfer functions*

The PLL is defined with three parameters, the cut-off frequency of the used filter f_{LPF}, the proportional feedback K_p and the intergral time T_i. Together, these parameters will determine how well the changes in the resonance frequency of the cantilever, and therefore changes in the input phase $\phi_i(t)$ can be followed. The frequency $f_r(t)$ that is set to minimize the error signal $\phi_\epsilon(t)$ can be extracted, and gives you the resonance frequency of the cantilever $f(t)$ as function of time. From $H_{closed}(\omega)$ we can determine for which frequencies the dynamics can be followed, in other words, we are interested in the bandwidth f_{BW} of the system.

In order to explain and analyse what determines the bandwidth of the system, $H_{closed}(\omega)$ is plotted in Fig. 2.11, together with the normalized error signal before the low pass filter, and $\Phi_\epsilon(\omega)/\Phi_i(\omega)$, the normalized error signal after the low pass filter. We choose parameters that resembles the parameters for the experiments in Ch. 5. Furthermore, we follow the procedure of the software of Zurich Instruments[34].

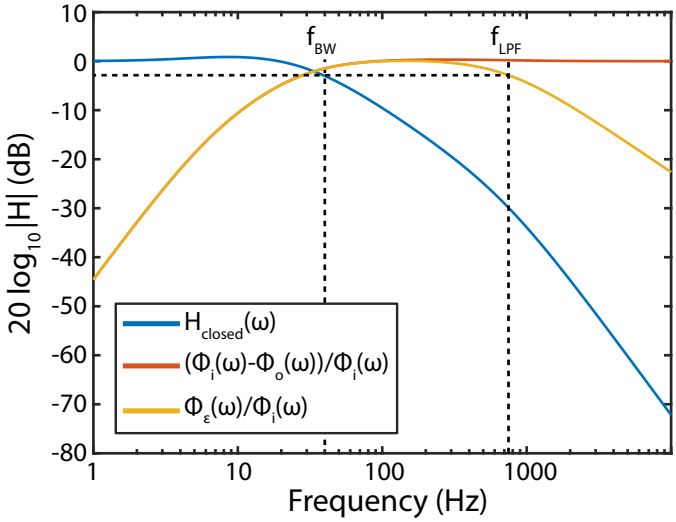

Figure 2.11: The Bode amplitude plots for the closed loop transfer function $H_{closed}(\omega)$ (Eq. 2.22), the normalized error signal before the low pass filter and the normalized error signal after the low pass filter $\Phi_\epsilon(s)$. In this example $T_i = 31.8$ ms, $K_p = 0.58$ Hz/degree and $f_{LPF} = 740$ Hz.

Firstly, Zurich Instruments chooses the integral time to equal the characteristic time scale for our mechanical resonator, $T_i = \frac{Q}{\pi f_0} = \frac{300}{\pi \times 3000 Hz} = 31.8$ ms[36]. Although this is a conventional choice for an amplitude controlled oscillator, we will show that in the case of a phase controlled oscillator the use of an integral feedback does not influence the bandwidth.

Secondly, the intended bandwidth is chosen by the user, in this example to be 40 Hz. The cut off frequency of the low pass filter f_{LPF} should not be too close around this bandwidth. The reason for this, is that otherwise the phase shift of the low pass filter makes the negative feedback circuit 'less' negative, and this makes $H_{closed}(\omega)$ less flat before the cut off frequency f_{BW}. A too high value for f_{LPF} makes the system more sensitive to noise. In this example, the choice of the software advisor is $f_{LPF} = 740$ Hz.

Finally, the last parameter K_p is chosen such that the desired bandwidth of 40 Hz is obtained, in this example this was in our case for $K_p = 0.58$ Hz/degree.

The result in Fig. 2.11 for $H_{closed}(\omega)$ is in perfect agreement with the result of the software Advisor, with taken into account the aforementioned factor of 2 in the proportional gain[34].

[36] Note that due to eddy currents, in Ch. 5 the quality factor is reduced to 300.

2.5.3 *The bandwidth of the phase locked loop*

Now we can ask ourselves what exactly determines the bandwidth of the system. Assume that we have a bandwidth $f_{BW} \ll f_{LPF}$, so that we can neglect the low pass filter. In this case the closed loop transfer function is given by:

$$H_{closed}(\omega) \approx \frac{1}{1 + \frac{i\omega}{360K_p}\left(\frac{1}{1+\frac{1}{i\omega T_i}}\right)} \tag{2.25}$$

Now we can distinguish two cases to simplify this function:

$$H_{closed}(\omega) \approx \begin{cases} \frac{1}{1+\frac{i\omega}{360K_p}} & \text{if } 360K_pT_i \gg 1 \text{ and } \omega \ll \omega_{BW} \\ \frac{1}{1-\frac{\omega^2 T}{360K_p}} & \text{if } 360K_pT_i \ll 1 \text{ and } \omega \ll \omega_{BW} \end{cases} \tag{2.26}$$

The bandwidth of the system is approximately given by the -3dB point of above equations. Note that for $360K_pT_i \ll 1$, the system is a second order system, with the resonance frequency $f_{unstable}$:

$$f_{unstable} = \frac{1}{2\pi}\sqrt{\frac{360K_p}{T_i}} \qquad \text{if } 360K_pT_i \ll 1 \tag{2.27}$$

Choosing your parameters such that the system becomes a second order system is highly unwanted, since we intent to have the PLL as flat as possible, so that the frequency $f_r(t)$ found with the PLL resembles the resonance frequency of the cantilever.

The software prevents above by ensuring that $360K_pT_i \gg 1$. In this case we find a bandwidth only determined by the proportional feedback:

$$f_{BW} = \frac{360}{2\pi}K_p \qquad \text{if } 360K_pT \gg 1 \tag{2.28}$$

To summarize, we have analyzed the PLL scheme including the software[34] we use to detect frequency shifts of our cantilever. We have found that the bandwidth of the PLL does not depend on the integral gain, but solely on the proportional gain. The bandwidth of the PLL gives the bandwidth at which you can detect changes in frequency. The noise in our scheme will be discussed in Ch. 5.

Bandwidth by Zurich Instruments lock-in

In the manual of Zurich Instruments (Zurich Instruments AG, 2016) it states: *"In general a larger ratio $\frac{K_p}{T_i}$ makes the PLL respond faster (i.e. it increases the bandwidth)."* Since the Advisor prevents the PLL to become a second order system, the statement in the manual is not fully correct, since the bandwidth is then only determined by K_p (Eq. 2.28)